CrystEngComm

Accepted Manuscript

ROYAL SOCIETY OF CHEMISTRY

www.rsc.org/crystengcomm

CrystEngComm

PAPER

The solvent effect on the structural and magnetic features of bidentate ligand-capped {Co$^{II}_9$[W^V(CN)$_8$]$_6$} Single-Molecule Magnets

Szymon Chorazy,[a,b] Anna Hoczek,[a] Maciej Kubicki,[c] Hiroko Tokoro,[b,d] Shin-ichi Ohkoshi,*[b,e] Barbara Sieklucka,[a] and Robert Podgajny*[a]

The cyanido-bridged {Co$^{II}_9$[W^V(CN)$_8$]$_6$} Single-Molecule Magnets grow spontaenously from the methanolic solution of Co^{2+} and [W^V(CN)$_8$]$^{3-}$ ions. Here, these molecules were combined with 2,2'-bipyridine N-oxide (2,2'-bpmo) ligand resulting in three novel crystalline phases: {Co^{II}[Co^{II}(2,2'-bpmo)(MeOH)]$_6$[Co^{II}(2,2'-bpmo)(MeCN)]$_2$[W^V(CN)$_8$]$_6$}·8H$_2$O·2MeCN·2MeOH (**1**) and {Co^{II}[Co^{II}(2,2'-bpmo)(MeOH)]$_8$[W^V(CN)$_8$]$_6$}·H$_2$O·8.5MeCN·11.5MeOH (**2**) growing from the MeOH-MeCN solution, and {Co^{II}[Co^{II}(2,2'-bpmo)(EtOH)]$_8$[W^V(CN)$_8$]$_6$}·3H$_2$O·5.5MeCN·5EtOH (**3**) crystallizing from the EtOH-MeCN mixture. They are constructed of {Co$^{II}_9$W$^V_6$} clusters of a six-capped body-centered cube topology, coordinating 2,2'-bpmo ligands at the external Co^{II} sites. **1-3** exhibit different composition and geometrical arrangement in the outer *fac*-[Co^{II}(μ-NC)$_3$(2,2'-bpmo)(solvent)]$^-$ moieties, and different solvent organization in the intercluster space. This results in a well pronounced geometrical isomerism of cluster cores being further related to the diverse non-covalent interaction schemes governing the supramolecular arrangement of molecules. **1**, **2**, and **3** reveal ferromagnetic coupling within Co-NC-W linkages leading to the high-spin ground state of 15/2, and slow magnetic relaxation at low temperatures. The single-molecule magnet characteristics are only slightly modulated by the solvent-dependent variation of structural features.

Introduction

The judicious combination of polycyanidometalates and d/f metal complexes with various organic or inorganic ligands gave rise to the series of molecular magnetic materials[1-6] which evolved towards magnetic sponges,[2b,7] photomagnets,[8] chiral magnets[9], and the systems combining magnetic phenomena with ferroelectricity,[10] ionic conductivity,[11] or luminescence.[12]

In this regard, the considerable attention is paid to polynuclear cyanido-bridged clusters.[3-4] They can combine a high spin in the ground state, up to the impressive value of S_{gr} = 45 found for the {Fe$_{42}$}[3d] cluster, with slow magnetic relaxation[4], and can reveal charge transfer or/and spin-crossover phenomena.[5a,13] They may also serve as the efficient molecular platforms for

the investigation of cyanido-mediated magnetic coupling.[14] All these features were shown to operate in the family of pentadecanuclear CN$^-$-bridged {M1^{II}[M1^{II}(L)$_3$]$_2$[M2^V(CN)$_8$]$_6$}, {M1$_9$M2$_6$} (M1 = Mn, Fe, Co, Ni; M2 = Mo, W, Re) molecules.[3a,15-18] Depending on the metal composition, they show the high spin ground state up to 39/2 for {Mn$_9$W$_6$},[3a] and slow magnetic relaxation as presented for {Co$_9$W$_6$}[15c,18c] and {Ni$_9$W$_6$} congeners.[17d] Very recently, we have discovered the charge transfer and spin transition effects in {Fe$_9$W$_6$},[16c] {Fe$_6$Co$_3$W$_6$},[16b] and {Fe$_9$Re$_6$}.[16d] As an important advantage, these clusters grow spontaneously from the methanolic or ethanolic solution containing M1^{2+} and [M2^V(CN)$_8$]$^{3-}$ ions. Moreover, they can be functionalized by various capping or bridging ligands through the substitution of solvent molecules coordinated primarily to the external M1 sites. Using this approach, our groups and others presented the range of diversely modified {M1$_9$M2$_6$} clusters,[17-18] including the construction of the cluster-based hybrid network with {Mn$_9$W$_6$} units linked both by cyanide and organic ligands.[18b]

During the last few years, we focused our attention on the {Co$_9$W$_6$} molecule, which was presented in 2005 as one of the first cyanido-bridged SMM.[15c] We have employed them as the Secondary Building Block in the syntheses of supramolecular and coordination chains. We have also combined them with chiral bidentate ligand producing the unique chiral SMM.[17f] Continuing this research pathway, we shifted our interest towards the investigation of the solvent effect on the

[a.] Faculty of Chemistry, Jagiellonian University, Ingardena 3, 30-060 Krakow, Poland. E-mail: robert.podgajny@uj.edu.pl
[b.] Department of Chemistry, School of Science, The University of Tokyo, 7-3-1 Hongo, Bunkyo-ku, Tokyo 113-0033, Japan E-mail: ohkoshi@chem.s.u-tokyo.ac.jp
[c.] Faculty of Chemistry, Adam Mickiewicz University, Umultowska 89b, 61-614 Poznań, Poland
[d.] Division of Materials Science, Faculty of Pure and Applied Sciences, University of Tsukuba, 1-1-1 Tennodai, Tsukuba, Ibaraki 305-8573, Japan
[e.] CREST, JST, K's Gobancho, Chiyoda-ku, Tokyo 102-0076, Japan

structural and magnetic characteristics of {Co$_9$W$_6$} molecules. The control of the structure and the resulting magnetism by the adjustment of solvent was presented for a number of cyanido-bridged assemblies, especially those revealing magnetic ordering with the critical temperature influenced by the guest solvent molecules.[7,9a] The solvent effect was also found to be the important factor in the structural and magnetic properties of Single Molecule Magnets, including the archetypal {Mn$_{12}$} and {Fe$_4$} molecules.[19]

In this context, we combined the bidentate 2,2'-dipyridyl N-oxide (2,2'bpmo) ligands with {Co$_9$W$_6$} clusters at various synthetic conditions employing four types of solvents: water, ethanol, methanol and acetonitrile. Here, we report the syntheses, crystal structures, and magnetic properties of three novel crystalline phases differing in the coordinated and crystallization solvent molecules: {Co[Co(2,2'-bpmo)(MeOH)]$_6$[Co(2,2'bpmo)(MeCN)]$_2$[W(CN)$_8$]$_6$}·8H$_2$O·2MeCN (**1**), {Co[Co(2,2'-bpmo)(MeOH)]$_8$[W(CN)$_8$]$_6$}·H$_2$O·8.5MeCN·11.5MeOH (**2**), and {Co[Co(2,2'-bpmo)(EtOH)]$_8$[W(CN)$_8$]$_6$}·H$_2$O·5.5MeCN·5EtOH (**3**). We discuss the solvent effect on the structural and magnetic features of these pseudo-polymorphic supramolecular isomers built of {Co$_9$W$_6$} clusters (**1-3**).

Experimental

Materials

The reagents Co^{II}Cl$_2$·6H$_2$O (Sigma-Aldrich), 2,2'-dipyridyl N-oxide (2,2'-bpmo, Sigma-Aldrich), and the solvents (acetonitrile = MeCN, ethanol = EtOH, methanol = MeOH) used in the syntheses were purchased from commercial sources. The cyanide precursors, Na$_3$[W^V(CN)$_8$]·4H$_2$O and TBA$_3$[W^V(CN)$_8$] (TBA = tetrabutylammonium cation), were prepared following the literature procedures.[20]

Syntheses and Basic Characterization of 1 – 3

Synthesis of 1. The 0.06 mmol (14.3 mg) portion of Co^{II}Cl$_2$·6H$_2$O, and 0.04 mmol (21.3 mg) of Na$_3$[W^V(CN)$_8$]·4H$_2$O were dissolved in 5 mL of MeOH/MeCN (1:1, v/v). Then, the freshly prepared solution of 2,2'-dipyridyl N-oxide (2,2'-bpmo, 0.06 mmol, 10.4 mg) in 5 mL of a MeOH – MeCN (1:1, v/v) was carefully added. The resulting deep red solution was stirred for several minutes, tightly closed, and transferred to a water bath with temperature of 30 °C. After a few days, the reasonable amount of red platelet crystals of **1** appeared, accompanied by the smaller amount of the second crystalline phase, that are red needle crystals of **2**. All attempts to separate these two phases by the modification of synthetic conditions were unsuccessful. Thus, the single crystals of **1** were mechanically separated from the crystals of **2**, and collected with the small amount of the mother solution. The crystals of **1** were identified as {Co^{II}[Co^{II}(2,2'-bpmo)(MeOH)]$_6$[Co^{II}(2,2'-bpmo)(MeCN)]$_2$[W^V(CN)$_8$]$_6$}·8H$_2$O·2MeCN·2MeOH by the single crystal X-ray diffraction analysis. This material was suitable for X-ray diffraction and other physical measurements in the mother solution, or protected by Apiezon N grease. Exposition of the crystals to the air leads to the hydrated form, **1hyd** with

the formula of {Co$^{II}_9$(2,2'-bpdo)$_8$[W^V(CN)$_8$]$_6$}·34H$_2$O as found in CHN analysis with the support of TGA and IR spectra. Yield: 10.2 mg, 31 %. CHN analysis of **1hyd**. Found: C, 31.7%; H, 2.55%; N, 18.4%. Calculated for Co$_9$W$_6$C$_{128}$H$_{132}$N$_{64}$O$_{42}$ (M = 4872.3 g·mol^{-1}): C, 31.6%; H, 2.73%; N, 18.4%. IR of **1hyd**. (KBr, cm^{-1}): 3405vs,br, O-H hydrogen bonding; 3127sh, 3094sh, 3066sh, ν(C-H); 2216vw, 2172w, 2148m, 2133sh, ν(C≡N); 1630s, δ(H$_2$O); 2,2'-bpmo: 1599s, 1576m, 1569m, 1505w, 1476s, 1444w, 1423, 1315w, 1302w, ν(C=C) and ν(C=N); 1273w, 1249w, 1234w, 1164m, 1124w, 1103w, 1075w, 1063w, 1041m, 1019m, 774s, 724m, 643m, 582m, 557m, δ(C-H), γ(C-H), aromatic rings deformations; 1204s, ν(N-O); 840m, bending N-O. TGA of **1hyd** (Figure S1): loss of 34 H$_2$O per {Co$_9$W$_6$} unit, calcd. 12.6 %, found 12.4 %.

Synthesis of 2. The solutions of Co^{II}Cl$_2$·6H$_2$O (3 mL, 14.3 mg, 0.06 mmol) and Na$_3$[W^V(CN)$_8$]·4H$_2$O (3 mL, 21.3 mg, 0.04 mmol) in a MeOH/MeCN (1:1, v/v) were stirred together for several minutes. Then, a solution of 2,2'-dipyridyl N-oxide (2,2'-bpmo, 0.06 mmol, 10.4 mg) in 6 mL of a MeOH/MeCN (1:1, v/v) mixture was added, and the resulting red solution was left for crystallization at room temperature. Red needle crystals of **2** appeared after a few days. The crystals of **2** were always accompanied by the small amount of the co-crystallizing red plates of **1** which could not be excluded by the modifications of the synthetic conditions. The crystals of **2** were mechanically separated from the crystals of **1**, and collected with the small amount of the mother solution.

The composition of **2**, {Co^{II}[Co^{II}(2,2'-bpmo)(MeOH)]$_8$[W^V(CN)$_8$]$_6$}·H$_2$O·8.5MeCN·11.5MeOH, was determined by the single crystal X-ray diffraction analysis. The crystalline phase of **2** was only stable in the mother solution, or covered by Apiezon N grease. Washing crystals with the solvent, and exposition to the air, lead to the hydrated form, **2hyd** with the composition of {Co$^{II}_9$(2,2'-bpdo)$_8$[W^V(CN)$_8$]$_6$}·36H$_2$O, as found in CHN analysis supported by TGA and IR spectra. Yield: 11.4 mg, 35 %. CHN analysis of **2hyd**. Found: C, 31.3%; H, 2.92%; N, 18.0%. Calculated for Co$_9$W$_6$C$_{128}$H$_{136}$N$_{64}$O$_{44}$ (M = 4908.3 g·mol^{-1}): C, 31.2%; H, 2.82%; N, 18.2%. IR (KBr, cm^{-1}): 3400vs,br, O-H hydrogen bonding; 3130sh, 3095sh, 3066sh, ν(C-H); 2218vw, 2174w, 2152m, 2134sh, ν(C≡N); 1629s, δ(H$_2$O). The 2,2'-bpmo-related peaks of **2hyd** in the 1600 – 550 cm^{-1} are, with the precision of ±2cm^{-1}, identical to those reported and interpreted above for **1hyd**. TGA of **2hyd** (Figure S1): loss of 36 H$_2$O per {Co$_9$W$_6$} unit, calcd. 13.2 %, found 12.9 %.

Synthesis of 3. The 0.1 mmol (23.8 mg) of Co^{II}Cl$_2$·6H$_2$O and 0.1 mmol (17.2 mg) of 2,2'-dipyridyl N-oxide (2,2'-bpmo) were dissolved together in the 8 mL of an EtOH/MeCN, (1:1, v/v). The resulting golden solution was mixed for 15 minutes, which was followed by the addition of TBA$_3$[W^V(CN)$_8$] (8 mL, 74.5 mg, 0.067 mmol) dissolved in an EtOH – MeCN (1:1, v/v) solvent. This resulted in the grey suspension which was stirred for 10 minutes, and left for crystallization at room temperature. Red block crystals of {Co^{II}[Co^{II}(2,2'-bpmo)(EtOH)]$_8$[W^V(CN)$_8$]$_6$}·3H$_2$O·5.5MeCN·5EtOH, **3** appeared from the grey precipitate after a few days. The composition of **3** was determined on the basis of X-ray structural analysis as this phase was suitable for physical measurements only in the mother liquor, or dispersed in

Apiezon N grease. Washing with the solvent, or exposition to the air, lead to the hydrated form, **3hyd** with the formula of $\{Co^{II}_9(2,2'\text{-bpdo})_8[W^V(CN)_8]_6\}\cdot 32H_2O$, as found by CHN analysis supported by TGA and IR spectra. Yield: 11.0 mg, 21 %. CHN analysis. Found: C, 32.1%; H, 2.81%; N, 18.3%. Calculated for $Co_9W_6C_{128}H_{128}N_{64}O_{40}$ (M = 4836.2 g·mol^{-1}): C, 31.8%; H, 2.67%; N, 18.5%. IR (KBr, cm^{-1}): 3400vs,br, O-H hydrogen bonding; 3128sh, 3097sh, 3069sh, ν(C-H); 2216vw, 2173w, 2149m, 2132sh, ν(C≡N); 1630s, δ(H$_2$O). The 2,2'-bpmo IR bands of **3hyd** are, with the precision of ±2cm^{-1}, identical to those reported above for **1hyd**. TGA of **3hyd** (Figure S1): loss of 32 H$_2$O per $\{Co_9W_6\}$ unit, calcd. 11.9 %, found 12.0 %.

Crystal Structure Determination

Single-crystal X-ray diffraction data of **1** were collected on an Agilent Technologies Xcalibur diffractometer with Eos CCD detector and graphite monochromated MoKα radiation, while the X-ray diffraction experiments for **2** and **3** were performed on a Rigaku R-AXIS RAPID diffractometer with an imaging plate area detector and graphite monochromated Mo Kα radiation. To prevent the loss of solvent molecules, single crystals were dispersed in Apiezon N grease, and measured at low temperature of 100 K. The crystal structure of **1** was solved by a direct method using SIR92,[21a] and refined by a full-matrix least-squares using SHELXL-2013.[21b] The crystal structures of **2** and **3** were solved and refined by the analogous methods using SHELXS-97, and SHELXL-2014/7, respectively (Table 1).[21b] Except of some disordered terminal cyanides and ethanol molecules in **3**, the non-hydrogen atoms of the clusters cores were refined anisotropically. The anisotropic refinement was also possible for non-hydrogen atoms of selected solvent molecules in **1** and **2**. Due to a structural disorder, only a part of hydrogen atoms in **1** and **2** were found independently, and refined isotropically. The positions of rest of hydrogen atoms in **1** and **2**, and of all hydrogen atoms in **3**, were calculated in the idealized positions, and refined isotropically using a riding model. The crystal structures of **1**-**3**, reveal a significant level of structural disorder. Thus, in order to maintain the proper geometries, and to ensure the convergence of the refinement process, a number of restraints on the bond lengths, angles (DFIX), and thermal ellipsoids (DELU, ISOR) were applied.

Table 1 Crystal data and structure refinement for **1** - **3**

compound	**1**	**2**	**3**
formula	$Co_{4.5}W_3C_{72}H_{62}N_{34}O_{12}$	$Co_9W_6C_{164.5}H_{169.5}N_{72.5}O_{28.5}$	$Co_9W_6C_{165}H_{164.5}N_{69.5}O_{24}$
formula weight / g·mol^{-1}	2412.29	5251.69	5138.62
T / K	100(1)	100(2)	100(2)
λ / Å	0.71073	0.71075	0.71075
crystal system	monoclinic	triclinic	monoclinic
space group	$P\,2_1/c$	$P\,\text{-}1$	$C\,c$
unit cell			
a / Å	20.2531(7)	19.0923(3)	19.4379(4)
b / Å	19.4998(4)	20.3195(4)	35.2593(9)
c / Å	29.3833(8)	31.5482(6)	30.9195(6)
α / deg	90	72.4270(10)	90
β / deg	122.990(3)	77.0630(10)	91.670(6)
γ / deg	90	68.6210(10)	90
V / Å^3	9733.4(5)	10775.3(4)	21182.2(8)
Z	4	2	4
calculated density / g·cm^{-3}	1.646	1.619	1.611
absorption coefficient / cm^{-1}	4.347	3.936	4.000
$F(000)$	4686	5158	10080
crystal size / mm × mm × mm	0.2 × 0.2 × 0.15	0.31 × 0.11 × 0.09	0.14 × 0.11 × 0.11
Θ range / deg	3.129 to 27.73	3.02 to 27.457	3.038 to 27.484
limiting indices	-25 < h < 26	-24 < h < 24	-24 < h < 25
	-25 < k < 24	-26 < k < 26	-45 < k < 45
	-38 < l < 36	-39 < l < 40	-40 < l < 40
collected reflections	100791	105628	100685
symmetry independent reflections	21256	48842	46872
R_{int}	0.1102	0.0307	0.0902
completeness / %	99.5	99.5	99.8
max and min transmission	0.477 and 0.562	0.375 and 0.718	0.604 and 0.667
data/restraints/parameters	21256/86/1192	48842/138/2919	46872/431/2207
GOF on F^2	1.060	1.044	1.183
final R indices	$R[F^2 > 2\sigma(F^2)] = 0.0855$	$R[F^2 > 2\sigma(F^2)] = 0.0371$	$R[F^2 > 2\sigma(F^2)] = 0.1070$
	$wR(F^2) = 0.2134$	$wR(F^2) = 0.0979$	$wR(F^2) = 0.2123$
largest diff peak and hole / e·Å^{-3}	3.88/-2.29	3.178/-1.796	3.083/-3.450

In particular, the restraints were used for (*i*) the bond lengths within the crystallization solvent molecules, and coordinated ethanol molecules in **3**, (*ii*) the bond lengths and thermal ellipsoids of some strongly disordered terminal cyanides in **1**-**3**, (*iii*) the thermal ellipsoids of carbon atoms of some disordered aromatic rings of 2,2'-bpmo ligands in **1**-**3**, and (*iv*) the C-H and O-H bond lengths for the part of independently found hydrogen atoms in **2**. Structural diagrams were prepared using Mercury 3.5.1. software.[21c] CCDC reference numbers are 1429836 (**1**), 1429837 (**2**), and 1429838 (**3**).

Physical Techniques

Infrared spectra were measured using JASCO FTIR-4100 spectrometer in the 4000 – 500 cm^{-1} range on crystals mixed and pressed with KBr. Thermogravimetric curves were measured on RIGAKU ThermoPlus TG8120 in the 20–375 °C range at a heating rate of 0.5 °C·min^{-1}. Powder diffraction data for polycrystalline samples of **1**-**3** sealed with the mother solution in glass capillary (0.5 mm of diameter), and of **1hyd**-**3hyd** also inserted in the glass capillary, were collected on a Rigaku SmartLab diffractometer using CuKα radiation, λ = 1.54425 Å, in the *2Θ* range of 3-40°, at room temperature. Magnetic measurements were performed on a Quantum Design 5T SQUID magnetometer. The magnetic data were collected on the grinded single crystals inserted in the glass tube with the small amount of the mother liquor. The obtained data were corrected for the diamagnetic contributions of both the compounds, and the solution using Pascal constants.[22] The diamagnetic contribution from the glass tube was also added.

Calculations

Continuous Shape Measure Analysis for the coordination spheres of eight-coordinated octacyanidotungstate(V) anions were performed using SHAPE software ver. 2.1.[23]

Results and discussion

Syntheses

The platelet crystals of **1**, and the needle crystals of **2** were obtained by the spontaneous crystallization from the MeCN/MeOH solution containing Co^{2+}, [W^V(CN)$_8$]$^{3-}$, and 2,2'-bpmo ligands. The domination of **1** or **2** in the synthetic mixture was achieved by the modification of concentrations and temperature while the composition of the MeCN/MeOH solvent mixture did not affect significantly the ratio between the amounts of phases **1** and **2** in the final product.

At higher concentrations, and increased temperature to ca. 30-35°C, the crystals of **1** repeatedly dominated. They were always accompanied by the small amount, ca. 2-5% of the crystals of **2**, which can be separated mechanically under an optical microscope. Lower concentration, and the room temperature conditions of ca. 20-25°C induced the dominance of the phase **2** with the only small admixture, ca. 5 % of the crystals of **1**, which could be separated and removed mechanically. All attempts to adjust the concentration and thermal conditions towards the pure phases of **1** or **2** were unsuccessful, thus, the dominant phase was always observed
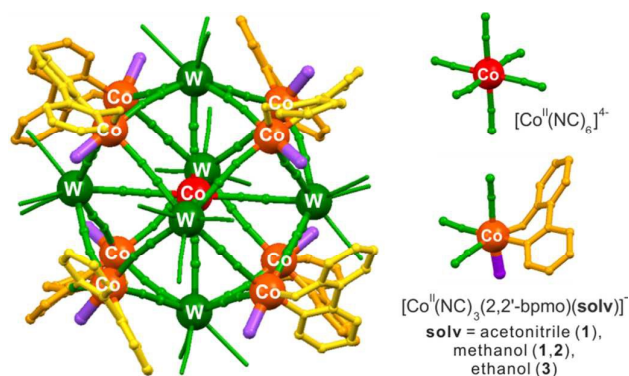

Figure 1. The general structural model of {Co^{II}[Co^{II}(2,2'-bpmo)(solvent)]$_8$[W^V(CN)$_8$]$_6$} clusters (left) in **1** (solvent molar ratio MeCN/MeOH = 1/3), **2** (solvent = MeOH), and **3** (solvent = EtOH) with the detailed insight into the ligands coordinated to the inner and to the external Co sites (right). Colours: cyanides = green, W = dark green, internal Co = red, external Co = deep orange, 2,2'-bpmo = yellow/orange, solvent = violet.

with the small impurity of the second phase. The reported final procedures were optimized in order to get the smallest amount of the minor phase.

The change of the solution to the MeCN/EtOH results in a single phase **3** that consists of red block crystals. Other combinations of solvents, including the application of propionitrile, acrylonitrile, and propanol did not produce the crystalline phases. That was also checked that the subtle change of the ratio between MeCN and MeOH/EtOH results in the same phases, **1**-**3**, while the excess of one of the solvent hampered the synthesis of any crystalline product.

Crystal structures

Molecular structures. Single crystals of **1**-**3** were characterized by X-ray diffraction analysis, and the resulting structures with crystal data are shown in Figures 1–3, S2–S10, and Tables 1, S1–S4. The structures of **1**-**3** consist of fifteen-centred cyanido-bridged {Co^{II}[Co^{II}(2,2'-bpmo)(solvent)]$_8$[W^V(CN)$_8$]$_6$} clusters of a six-capped body-centred cubic topology,[17] and intercluster solvent molecules. The cluster core, built of nine Co^{II} and six W^V centers, is capped by eight N,O-bidentate 2,2'-bpmo ligands, and eight solvent molecules coordinated by external Co^{II} sites (Figure 1). As a result, the clusters in **1**-**3** reveal one inner [Co^{II}(μ-NC)$_6$]$^{4-}$ unit, and eight outer *fac*-[Co^{II}(μ-NC)$_3$(2,2'-bpmo)(solvent)]$^-$ moieties, notably with different solvent composition, and the related {N$_x$O$_y$} coordination modes (Figure 2). In **1**, two MeCN molecules are capping the cluster core taking the positions on the opposite corners of the Co-based cube, while the remaining six places are occupied by MeOH. In **2**, all solvent positions on external Co^{II} complexes are occupied by MeOH, while for **3**, EtOH molecules are coordinated to Co^{II}. Due to the change of the space group from *P*2$_1$/c to *P*-1, and *C*c on going from **1** to **2**, and **3**, the crystal structure of **2** contains two cluster units (A and B) differing in the detailed structural parameters, while only one type of cluster is presented for **1** and **3** (Figure 2, Tables S1–S3). Consequently, the asymmetric units are different in **1**-**3** (Figures S2–S4, and description in the Supporting Information), and they include different amounts of crystallization H$_2$O,
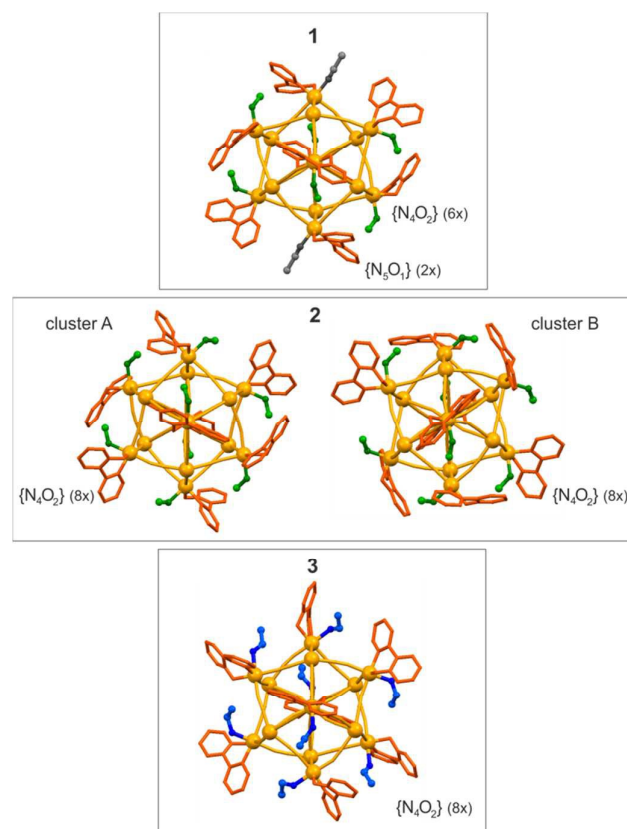
Figure 2. Arrangements of capping ligands on the surface of $\{Co^{II}_9W^{V}_6\}$ clusters in **1**, **2** (clusters A and B), and **3**, with the emphasized Co coordination modes. The terminal cyanides and hydrogen atoms were omitted for clarity. Colours: cluster skeleton – yellow, 2,2'-bpmo – orange, MeCN – grey, MeOH – green, EtOH – blue.

Figure 3. Isomeric forms of $\{Co^{II}[Co^{II}(2,2'\text{-bpmo})(solvent)]_8[W^{V}(CN)_8]_6\}$ clusters existing in **1**, **2** (clusters A and B), and **3** (top), and the general model of the geometrical isomer representing all these clusters for the case of indistinguishable donor atoms (bottom). Colours: cluster skeleton – grey, nitrogen of 2,2'-bpmo or MeCN – blue, oxygen of 2,2'-bpmo, EtOH, or MeOH – red. The yellow background represents the parts which are common for three of four depicted clusters. For clarity only one half of each cluster was shown.

MeOH and MeCN molecules in **1** and **2**, and a number of H_2O, MeCN and EtOH molecules in **3**. Their detailed structural parameters, including the bond lengths and angles within the Co^{II} and W^{V} complexes, are depicted in Tables S1, S2, and S3, respectively. They show the differences not only between the compounds **1–3** but also between the A and B types of clusters in **2**. In effect, the $[W(CN)_8]^{3-}$ moieties in **1-3** form three distinct polyhedral sets, including a dodecahedron (DD-8) case and a mixed DD-8/BTP-8/SAPR-8 geometry between DD-8, a bicapped trigonal prism (BTP-8), and a square antiprism (SAPR-8). This was shown by a Continuous Shape Measure Analysis, and discussed in the Supporting Information (Table S4).

Geometrical isomerism. The clusters of **1-3** differ in the spatial arrangement of terminal ligands coordinated to external Co^{II} sites (Figure 2). The alignment of 2,2'-bpmo ligands varies depending on the solvent attached to Co^{II}. It is also noticeably different for the A and B clusters of **2**. This can be explained by the detailed analysis of the geometrical isomerism of $\{Co^{II}[Co^{II}(2,2'\text{-bpmo})(solvent)]_8[W^{V}(CN)_8]_6\}$ clusters existing in **1**, **2** (clusters A and B), and **3** (Figure 3). Considering the case of indistinguishable donor atoms, the clusters of **1-3** exhibit the same isomer of the C_i symmetry, according to the classification given by B. Nowicka et al.[17e] However, the N,O-mixed coordination of 2,2'-bpmo, and the N or O coordination of the solvents decrease the symmetry, and a number of various
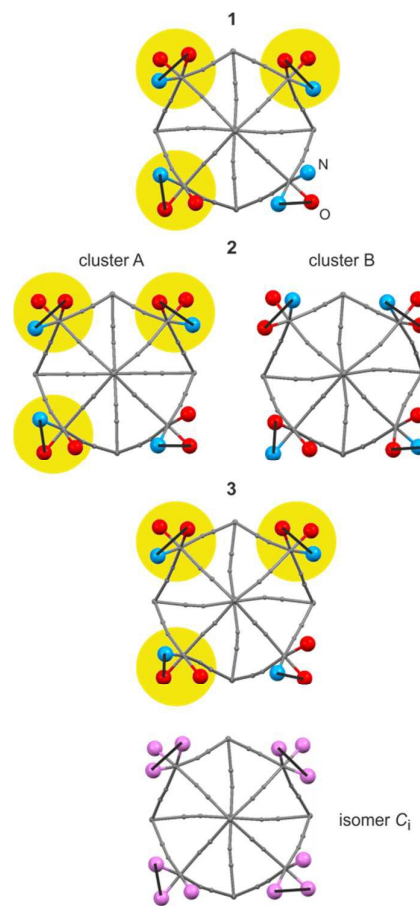
isomers can be achieved. Interestingly, three types of clusters of **1**, **2** (A), and **3** reveal analogous arrangement of donor atoms on three of four indicated positions (distinguished by the yellow areas in the Figure 3). Among them, the cluster A of **2**, and the cluster **3** exhibit exactly the same isomer confirming the identical alignment of 2,2'-bpmo and solvent ligands. The cluster of **1** shows the different arrangements of donor atoms for one type of Co, contributing to the subtle differences in the spatial arrangement of ligands, while the geometrical isomer, and the resulting ligands' arrangement is unique for the cluster B of **2**.

Supramolecular architectures. **1-3** present the distinct supramolecular arrangements of clusters due to the various types of non-covalent interactions (Figures S5–S7). In **1**, two types of intercluster contacts within the crosswise (100) and (10-2) planes are observed (Figure S5). The interactions within (100) plane (TYPE 1) are dominated by the π-π interaction between aromatic rings of 2,2'-bpmo which is supported by the hydrogen bonds involving hydroxyl group of coordinated MeOH of the first cluster, and the O⁻ anion of 2,2'-bpmo of the

neighbouring molecule. This cooperation of π-π and hydrogen bonds was achieved only between the pairs of external Co sites employing the Co^{II} complex with coordinated MeCN. Thus, the interactions within the (10-2) plane (TYPE 2), are much weaker, and consist only on π-π interactions between 2,2'-bpmo ligands. The supramolecular alignment of the $\{Co_9W_6\}$ molecules in **2** involves two geometrical types of clusters (Figure S6). The main interactions were detected between A and B clusters within (011) and (110) planes, and the additional contacts entangling only B clusters are spread over the (001) plane. Within (011) plane, the π-π interaction of 2,2'-bpmo coordinated to Co4 and Co7 is observed (TYPE 2), which is supported by the hydrogen bonds involving MeOH of Co2, non-coordinated MeOH, and terminal cyanides of W6 (TYPE 1). The partial π-π interactions between 2,2'-bpmo of Co5 and Co8 are observed within (110) plane (TYPE 3), which is accompanied by the exotic π-π contacts involving the pyridine rings of Co3 and Co8, and the π-bonding system of non-coordinated MeCN stacked between them (TYPE 4). The interactions within (001) plane consists of π-π interaction between 2,2'-bpmo of Co9 centers (TYPE 6), and the weak hydrogen bonding system employing terminal cyanides of W4, and C-H groups of aromatic rings belonging to the Co6 complex (TYPE 5). The π-π interactions strongly dominate in the intercluster contacts detected in **3** (Figure S7). They are observed within the (001) plane between 2,2'-bpmo ligands coordinated to Co4–Co8 (TYPE 1), and Co3–Co7 (TYPE 2) pairs, and within (100) plane involving Co2–Co6 (TYPE 3) pairs. In addition, within (010) plane, there is a weak hydrogen bonding system between terminal cyanides of W3 and W6, and C-H groups of 2,2'-bpmo of Co9 and Co5, respectively.

As a result of non-covalent interactions, **1**-**3** reveal different intermetallic distances of the neighbouring clusters. In **1**, the shortest intercluster distance is 6.0 Å between Co3 and Co5 which is due to the π-π and hydrogen bonding interactions (TYPE 1, Figure S5). Much longer intercluster distances are detected for **2**, with the shortest value of 7.9 Å for Co4–Co7 neighbours interacting through π-π interaction (TYPE 2, Figure S6). The identical shortest distance of 7.9 Å found for Co3–Co7 pairs of **3** is related to the respective π-π interactions of TYPE 2 (Figure S7). The intercluster space in **1**-**3** is filled by a number of crystallization solvent molecules. In **1**, both the interstitial H_2O, MeCN and MeOH molecules were detected, and they are aligned between clusters within *bc* plane (Figure S8). **2** reveals the identical types of solvent but with the overwhelming amount of MeCN and MeOH. These molecules are arranged within (011) plane (Figure S9). In **3**, EtOH accompanied by the smaller amounts of MeCN and H_2O were detected. They fill the channels along *c* direction but the part of them were also found within *ab* plane (Figure S10).

Powder X-ray diffraction studies

Powder X-ray diffraction (PXRD) measurements of **1**-**3** were performed on the polycrystalline samples covered by the mother liquid, and inserted into the glass capillary. The experimental diffraction patterns correspond well to the patterns calculated on the basis of the respective structural

models found in the single-crystal studies (Figure S11). This indicates a good purity of the obtained phases, and the validity of the structural model for the bulk samples used in the magnetic measurements.

The powder diffraction patterns were also measured for the hydrated forms of **1**, **2**, and **3**, called **1hyd**, **2hyd**, and **3hyd**, respectively (Figure S12), which were obtained after removal of the crystals from the solution, and air-drying to the stable composition. The resulting air-stable polycrystalline solids are characterized by the formula of $\{Co^{II}_9(2,2'\text{-bpdo})_8[W^V(CN)_8]_6\}$·$nH_2O$, where n = 34 for **1hyd**, n = 36 for **2hyd**, and n = 32 for **3hyd**, as determined by CHN elemental analysis confronted with the thermogravimetric analysis, and IR spectra showing the presence of water as the only solvent for **1hyd**-**3hyd** phases (see Experimental section). The PXRD patterns of **1hyd**-**3hyd** are visibly different from the as-synthesized **1**-**3** phases. This can be explained by the change of the solvent from the H_2O/MeOH/EtOH-MeCN mixture to the purely water content which presumably results in the re-arrangement of the cyanido-bridged clusters. Due to the low symmetry, and the decreased crystallinity upon drying, the crystal structures of **1hyd**-**3hyd** could not be determined. However, the Rietveld analyses performed for the representative low angles ranges enabled to estimate the cell parameters of **1hyd**-**3hyd** (Figure S12, Table S5). When compared with the corresponded PXRD patterns of **1**-**3** measured at the identical temperature of 298 K, the hydrated forms, **1hyd**-**3hyd** reveal the significant contraction of the unit cell from 10050 to 8709 Å^3 (ca. 13% of the decrease), 11242 to 8315 Å^3 (ca. 26%), and 22203 to 17102 Å^3 (ca. 23%) for **1hyd**, **2hyd**, and **3hyd**, respectively.

Magnetic properties

The *dc* magnetic properties of **1**, **2**, and **3**, including the temperature dependence of molar magnetic susceptibility, $\chi_M T(T)$ in the 1.8–300 K range, and the field dependence of magnetization, $M(H)$ at T = 1.8 K are presented in Figure 4. Room temperature $\chi_M T$ values for $\{Co^{II}_9W^V_6\}$ unit of **1**, **2**, and **3** are 33.6, 33.7, and 33.9 cm^3 mol^{-1} K, respectively, which are close to the limit of the 27–33 cm^3 mol^{-1} K range predicted for combined contributions from the isolated six W^V (S_W = 1/2, g_W = 2.0), and nine Co^{II} (S_{Co} = 3/2, g_{Co} = 2.4–2.7).[24] Upon cooling, the $\chi_M T$ gradually increases to the maximum of 70.1, 67.8, and 71.1 cm^3 mol^{-1} K at 5.6, 6.4, and 4.5 K for **1**, **2**, and **3**, respectively, indicating the ferromagnetic interactions within the Co–NC–W linkages (Figure 4a). This is followed by the further decrease of $\chi_M T$ to 50.5 (**1**), 55.1 (**2**), and 62.6 (**3**) cm^3 mol^{-1} K at 1.8 K, which can be ascribed to antiferromagnetic intercluster correlation, and zero-field splitting effects on Co^{II}. The maxima of $\chi_M T$ agrees moderately well with the limit of 92 cm^3 mol^{-1} K calculated for the ferromagnetic ground state of S_F = 15/2 with g_{av} = 3.4 of $\{Co^{II}_9W^V_6\}$ cluster when the standard parameters of W^V (S_W = 1/2, g_W = 2.0), and the effective spin approach of Co^{II} ($S_{Co,LT}$ = 1/2, $g_{Co,LT}$ = 4.3) are taken into account.[24] The ferromagnetic type of interactions is, however, strongly supported by the $M(H)$ plots showing the fast increase to 26.4 (**1**), 27.1 (**2**), and 25.9 (**3**) Nβ at H = 50 kOe, which are only slightly higher than the expected 25.5 Nβ (Figure 4b).
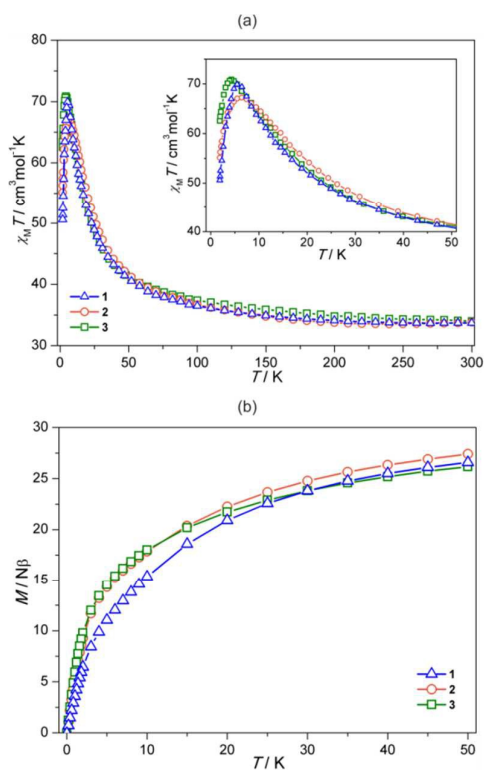
Figure 4. *Dc* magnetic properties of **1**, **2**, and **3**: (a) $\chi_M T(T)$ plots in the 1.8 – 300 K range measured at *H* = 1 kOe with the enlargement of the 1.8 – 50 K region in the inset, and (b) the field dependences of magnetization at *T* = 1.8 K.

Due to the presence of anisotropic Co^{II} implemented into the high spin molecule, both **1**, **2**, and **3** reveal the frequency dependent *ac* magnetic susceptibility suggesting the onset of slow magnetic relaxation characteristic of SMMs (Figures 5 and S13). However, it occurs at very low temperatures, and the maxima of $\chi_M''(T,\nu)$ could not be detected, even with the applied *dc* fields (Figure S14). Despite this, the low temperature *ac* susceptibility at various frequencies was successfully analysed using a generalized Debye model for the fitting of the Cole–Cole plots (Figure S13). The resulting average α parameters are 0.35(5), 0.26(4), and 0.17(4) for **1**, **2**, and **3**, respectively, suggesting rather broad, and the solvent-dependent distribution of relaxation times. The α parameters were furtheral used in the rough estimation of average energy barrier ΔE, which was found from the linear fitting of $\ln(\chi_M''/\chi_M')$ versus T^{-1} plots as their slope is equal to $\Delta E(1-\alpha)/k_B$ (k_B = Boltzmann constant, Figure 5). This method, assuming a single Arrhenius relaxation, has been already used for the approximation of the energy barrier in the {Co$^{II}_9$W$^{V}_6$} clusters (for details, see Supporting Information and ref. 17f). The values of $\Delta E/k_B$ and τ_0 are collected in Table 2. **1**-**3** reveal very similar level of the energy barriers between 10 and 11 K which is accompanied by the τ_0 values of 1.7–3.6·10^{-8} s. These values are within the range characteristic of SMMs.[1f,4] They are close to the parameters obtained for reported {Co$^{II}_9$W$^{V}_6$} clusters, however, the energy barrier is decreased when compared with the original, purely solvated {Co$^{II}_9$W$^{V}_6$} SMM.[15c]
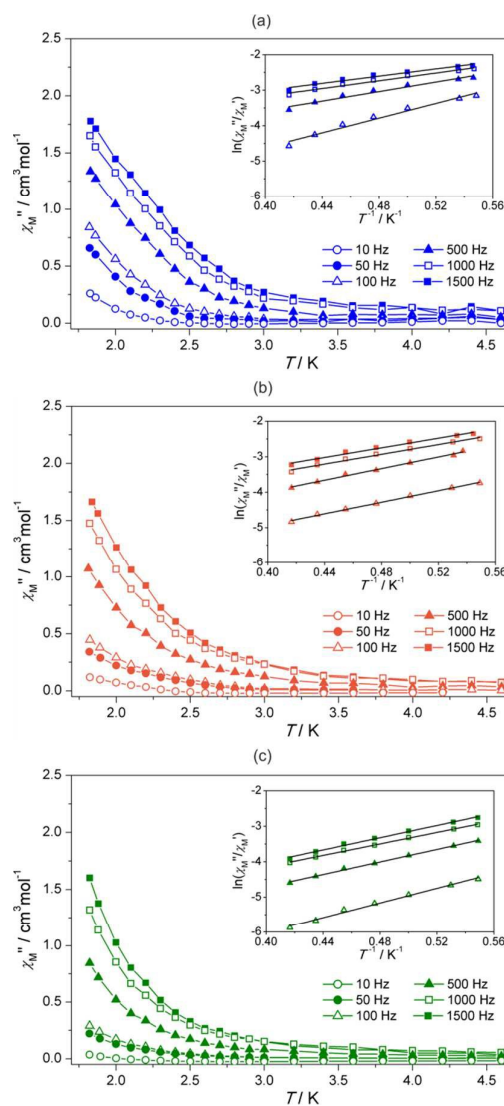

Figure 5. Temperature dependences of out-plane component of *ac* magnetic susceptibility, χ_M'' at various indicated frequencies together with the $\ln(\chi_M''/\chi_M')$ plots in the insets for **1** (a), **2** (b), and **3** (c). Experimental conditions: H_{ac} = 3 Oe, H_{dc} = 0 Oe.

Comparing the magnetic curves gathered in Figures 4–5, and the parameters of *ac* dynamics presented in Table 2, it is seen that the solvent-dependent variation of structural features only weakly affects the magnetic characteristics. All of the clusters reveal the ferromagnetic ground spin state. The subtle differences in the $\chi_M T(T)$ and *M(H)* plots are probably related to the small differences in metric parameters influencing the strength of intramolecular magnetic coupling. This super-imposes with the changes in the intercluster contacts between **1**, **2**, and **3** affecting the intermolecular antiferromagnetic correlation. The dynamic parameters of slow magnetic relaxation are similar for **1**, **2**, and **3**, indicating that the solvent on the sixth position on Co^{II} plays only the minor role in the overall anisotropy of the cluster. The highest energy barrier, and the longest relaxation time is ascribed, however, to **1** exhibiting the anisotropic arrangement of solvents with MeCN

aligned along the one distinguished direction (Figure 2). This is in line with the previous findings on the $\{M1_9M2_6\}$ molecules showing that the anisotropic arrangement of the capped ligands can be of crucial importance to enhance the SMM characteristics.[17d,25] On the other hand, the value of ΔE could be here also affected by the fact of a relatively close intercluster contacts, ranging from 6–8 Å for **1**–**3**.

Table 2. Summary of *ac* magnetic dynamics of **1**, **2**, **3**, and other reported $\{Co^{II}_9W^V_6\}$ molecules revealing slow relaxation of magnetization

Compound	$\Delta E/k_B$ (K)	τ_0 / s	Ref.
1	11(2)	$3.6(12)\cdot10^{-8}$	this work
2	10.1(11)	$3.3(9)\cdot10^{-8}$	
3	10.7(14)	$1.7(6)\cdot10^{-8}$	
$\{Co_9(MeOH)_{24}[W(CN)_8]_6\}\cdot19H_2O$	27.79^a	$7.39\cdot10^{-11}$	15c
$\{Co_9(R\text{-mpm})_8(MeOH)_8[W(CN)_8]_6\}$ $\cdot14MeOH$	$19(4)^b$	$4(2)\cdot10^{-9}$	17f
$\{Co_9(MeOH)_{24}[W(CN)_8]_6\}$ $\cdot4,4'\text{-bpdo}\cdot MeOH\cdot H_2O$	$10.3(5)^a$	$4(1)\cdot10^{-9}$	18c

^{a}Obtained from the positions of peaks in the $\chi''(T)$ plots. ^{b}Obtained from the the $\ln(\chi''/\chi')(T^{-1})$ plots supported by the Cole – Cole $\chi''(\chi')$ plots, as for **1**, **2**, and **3**. Abbreviations: 4,4'-bpdo = 4,4'-bipyridine N,N'-dioxide; R-mpm = (R)-α-methyl-2-pyridinemethanol.

Conclusions

We report three novel crystalline phases based on the pentadecanuclear $\{Co^{II}_9[W^V(CN)_8]_6\}$ clusters capped by N,O-bidentate 2,2'-bipyridine N-oxide (2,2'-bpmo) which exhibit significant structural differences related to the coordination and crystallization of solvent molecules (H_2O, MeOH, EtOH and MeCN). This is best illustrated by the different composition of crystallization solvent molecules, geometrical isomerism of the cluster cores, domination of different types of non-covalent interactions, and the resulting supramolecular arrangement of the clusters governing the intercluster distances. All of the $\{Co^{II}_9[W^V(CN)_8]_6\}$ molecules in **1**, **2**, and **3** reveal the cyanide-mediated Co^{II}–W^V ferromagnetic coupling leading to the ferromagnetic ground state of 15/2, and to the slow magnetic relaxation effect characteristic of Single-Molecule Magnets (SMMs). The SMM behaviour is, however, weakened when compared with the purely solvated $\{Co_9(MeOH)_{24}[W(CN)_8]_6\}$ $\cdot19H_2O$. The magnetic properties were found to be only subtly sensitive to the solvent-dependent variation of the intracluster and supramolecular features of **1**, **2**, and **3**. However, the unique anisotropic arrangement of the MeCN and MeOH solvents on the surface of $\{Co_9W_6\}$ clusters in **1** gave the most pronounced characteristics. This suggests that induction of the anisotropic alignment of ligands coordinated to the external Co sites can be a promising route towards the $\{Co_9W_6\}$-based Single Molecule Magnets with higher values of the energy barrier. This could be achieved by the smaller than eight number of coordinated bidentate ligands, or by the implementation of two types of capping molecules. We are now checking these possibilities in our laboratory.

Notes and references

1   (*a*) M. Verdaguer and G. Girolami, in *Magnetism – Molecules to Materials*, ed. J. S. Miller and M. Drillon, Wiley-VCH, 2004, vol. 5, pp. 283–346; (*b*) J. S. Miller, *Chem. Soc. Rev.*, 2011, **40**, 3266; (*c*) H. Tokoro and S. Ohkoshi, *Dalton Trans.*, 2011, **40**, 6825; (*d*) X.-Y. Wang, C. Avendano and K. R. Dunbar, *Chem. Soc. Rev.*, 2011, **40**, 3213; (*e*) B. Nowicka, T. Korzeniak, O. Stefańczyk, D. Pinkowicz, S. Chorazy, R. Podgajny, B. Sieklucka, *Coord. Chem. Rev.*, 2012, **256**, 1946; (*f*) K. S. Pedersen, J. Bendix, R. Clerac, *Chem. Commun.*, 2014, **50**, 4396.

2   (*a*) S. M. Holmes and G. S. Girolami, *J. Am. Chem. Soc.*, 1999, **121**, 5593; (*b*) S. Tanase, F. Tuna, P. Guionneau, T. Maris, G. Rombaut, C. Mathoniére, M. Andruh, O. Kahn and J.-P. Sutter, *Inorg. Chem.*, 2003, **42**, 1625; (*c*) K. Imoto, M. Takemura, H. Tokoro and S. Ohkoshi, *Eur. J. Inorg. Chem.* 2012, 2649.

3   (*a*) Z. J. Zhong, H. Seino, Y. Mizobe, M. Hidai, A. Fujishima, S. Ohkoshi, and K. Hashimoto, *J. Am. Chem. Soc.*, 2000, **122**, 2952; (*b*) L. M. C. Beltran and J. R. Long, *Acc. Chem. Res.*, 2005, **38**, 325; (*c*) X.-Y. Wang, A. V. Prosvirin and K. R. Dunbar, *Angew. Chem. Int. Ed.*, 2010, **49**, 5013; (*d*) S. Kang, H. Zheng, T. Liu, K. Hamachi, S. Kanegawa, K. Sugimoto, Y. Shiota, S. Hayami, M. Mito, T. Nakamura, M. Nakano, M. L. Baker, H. Nojiri, K. Yoshizawa, C. Duan and O. Sato, *Nat. Commun.*, 2014, **6**: 5955.

4   (*a*) J. J. Sokol, A. G. Hee and J. R. Long, *J. Am. Chem. Soc.*, 2002, **124**, 7656; (*b*) E. J. Schelter, F. Karadas, C. Avendano, A. V. Prosvirin, W. Wernsdorfer and K. R. Dunbar, *J. Am. Chem. Soc.*, 2007, **129**, 8139; (*c*) D. E. Freedman, D. M. Jenkins, A. T. Iavarone and J. R. Long, *J. Am. Chem. Soc.*, 2008, **130**, 2884.

5   (*a*) M. G. Hilfiger, M. Chen, T. V. Brinzari, T. M. Nocera, M. Shatruk, D. T. Petasis, J. L. Musfeldt, C. Achim and K. R. Dunbar, *Angew. Chem. Int. Ed.*, 2010, **49**, 1410; (*b*) N. Ozaki, H. Tokoro, Y. Hamada, A. Namai, T. Matsuda, S. Kaneko, S. Ohkoshi, *Adv. Funct. Mater.*, 2012, **22**, 2089; (*c*) N. Hoshino, F. Iijima, G. N. Newton, N. Yoshida, T. Shiga, H. Nojiri, A. Nakao, R. Kumai, Y. Murakami and H. Oshio, *Nat. Chem.*, 2012, **4**, 921; (*d*) B. Nowicka, M. Reczyński, M. Rams, W. Nitek, J. Żukrowski, C. Kapusta and B. Sieklucka, *Chem. Commun.*, 2015, **51**, 11485.

6   (*a*) M. Seredyuk, A. B. Gaspar, V. Ksenofontov, Y. Galyametdinov, M. Verdaguer, F. Villain and P. Gütlich, *Inorg. Chem.*, 2010, **49**, 10022; (*b*) M. Carmen Munoz and J. A. Real, *Coord. Chem. Rev.*, 2011, **255**, 2068; (*c*) S. Ohkoshi, K. Imoto, Y. Tsunobuchi, S. Takano and H. Tokoro, *Nat. Chem.*, 2011, **3**, 564; (*d*) A. Mondal, Y. Li, L.-M. Chamoreau, M. Seuleiman, L. Rechignat, A. Bousseksou, M.-L. Boillot and R. Lescouëzec, *Chem. Commun.*, 2014, **50**, 2893; (*e*) *Spin-Crossover*

Materials: Properties and Applications, ed. M. A. Halcrow, Wiley-VCH, Oxford, 2013.

7 (*a*) J. Milon, M.-C. Daniel, A. Kaiba, P. Guionneau, S. Brandés and J.-P. Sutter, *J. Am. Chem. Soc.*, 2007, **129**, 13872; (*b*) D. Pinkowicz, R. Podgajny, B. Gaweł, W. Nitek, W. Łasocha, M. Oszajca, M. Czapla, M. Makarewicz, M. Bałanda and B. Sieklucka, *Angew. Chem. Int. Ed.*, 2011, **50**, 3973; (*c*) B. Nowicka, M. Reczyński, M. Rams, W. Nitek, M. Kozieł and B. Sieklucka, *CrystEngComm*, 2015, **17**, 3526.

8 (*a*) S. Ohkoshi, H. Tokoro, *Acc. Chem. Res.*, 2012, **45**, 1749; (*b*) E. S. Koumousi, I.-R. Jeon, Q. Gao, P. Dechambenoit, D. N. Woodruff, P. Merzeau, L. Buisson, X. Jia, D. Li, F. Volatron, C. Mathoniere, R. Clerac, *J. Am. Chem. Soc.*, 2014, **136**, 15461 – 15464.; (*c*) C. R. Gros, M. K. Peprah, B. D. Hosterman, T. V. Brinzari, P. A. Quintero, M. Sendova, M. W. Meisel and D. R. Talham, *J. Am. Chem. Soc.*, 2014, **136**, 9846.

9 (*a*) D. Pinkowicz, R. Podgajny, W. Nitek, M. Rams, A. M. Majcher, T. Nuida, S. Ohkoshi and B. Sieklucka, *Chem. Mater.*, 2011, **23**, 21; (*b*) S. Chorazy, R. Podgajny, W. Nitek, T. Fic, E. Görlich, M. Rams and B. Sieklucka, *Chem. Commun.*, 2013, **49**, 6731; (*c*) S. Ohkoshi, S. Takano, K. Imoto, M. Yoshikiyo, A. Namai and H. Tokoro, *Nat. Photon*., 2014, **8**, 65.

10 (*a*) S. Ohkoshi, H. Tokoro, T. Matsuda, H. Takahashi, H. Irie and K. Hashimoto, *Angew. Chem. Int. Ed.*, 2007, **46**, 3238; (*b*) C.-F. Wang, D.-P. Li, X. Chen, X.-M. Li, Y.-Z. Li, J.-L. Zuo and X.-Z. You, *Chem. Commun.*, 2009, 6940.

11 S. Ohkoshi, K. Nakagawa, K. Tomono, K. Imoto, Y. Tsunobuchi and H. Tokoro, *J. Am. Chem. Soc.*, 2010, **132**, 6620.

12 (*a*) E. Chelebaeva, J. Larionova, Y. Guari, R. A. S. Ferreira, L. D. Carlos, F. A. Almeida Paz, A. Trifonov and C. Guerin, *Inorg. Chem.*, 2009, **48**, 5983; (*b*) S. Chorazy, K. Nakabayashi, S. Ohkoshi and B. Sieklucka, *Chem. Mater.*, 2014, **26**, 4072.

13 (*a*) M. Shatruk, A. Dragulescu-Andrasi, K. E. Chambers, S. A. Stoian, E. L. Bominaar, C. Achim and K. R. Dunbar, *J. Am. Chem. Soc.*, 2007, **129**, 6104; (*b*) Y. Zhang, D. Li, R. Clerac, M. Kalisz, C. Mathoniere and S. M. Holmes, *Angew. Chem. Int. Ed.*, 2010, **122**, 3840; (*c*) N. Bridonneau, J. Long, J.-L. Cantin, J. von Bardeleben, S. Pillet, E.-E. Bendeif, D. Aravena, E. Ruiz and V. Marvaud, *Chem. Commun.*, 2015, **51**, 8229.

14 (*a*) K. E. Vostrikova, D. Luneau, W. Wernsdorfer, P. Rey and M. Verdaguer, *J. Am. Chem. Soc.*, 2000, **122**, 718; (*b*) J.-N. Rebilly, L. Catala, E. Riviere, R. Guillot, W. Wernsdorfer and T. Mallah, *Inorg. Chem.*, 2005, **44**, 8194; (*c*) K. E. Funck, M. G. Hilfiger, C. P. Berlinguette, M. Shatruk, W. Wernsdorfer and K. R. Dunbar, *Inorg. Chem.*, 2009, **48**, 3438.

15 (*a*) J. Larionova, M. Gross, M. Pilkington, H. Andres, H. Stoeckli-Evans, H. U. Güdel and S. Decurtins, *Angew. Chem. Int. Ed.*, 2000, **39**, 1605; (*b*) F. Bonadio, M. Gross, H. Stoeckli-Evans and S. Decurtins, Inorg. Chem., 2002, **41**, 5891; (*c*) Y. Song, P. Zhang, X.-M. Ren, X.-F. Shen, Y.-Z. Li and X.-Z. You, *J. Am. Chem. Soc.*, 2005, **127**, 3708; (*d*) S.-L. Ma, S. Ren, Y. Ma, D.-Z. Liao and S.-P. Yan, *Struct. Chem.*, 2009, **20**, 161.

16 (*a*) D. E. Freedman, M. V. Bennett and J. R. Long, *Dalton Trans.*, 2006, 2829; (*b*) R. Podgajny, S. Chorazy, W. Nitek, M. Rams, A. M. Majcher, B. Marszałek, J. Żukrowski, C. Kapusta and B. Sieklucka, *Angew. Chem. Int. Ed.*, 2013, **52**, 896; (*c*) S. Chorazy, R. Podgajny, W. Nogaś, W. Nitek, M. Kozieł, M. Rams, E. Juszyńska-Gałązka, J. Żukrowski, C. Kapusta, K. Nakabayashi, T. Fujimoto, S. Ohkoshi and B. Sieklucka, *Chem. Commun.*, 2014, **50**, 3484; (*d*) S. Chorazy, R. Podgajny, K. Nakabayashi, J. Stanek, M. Rams, B. Sieklucka and S. Ohkoshi, *Angew. Chem. Int. Ed.*, 2015, **54**, 5093.

17 (*a*) J. H. Lim, J. H. Yoon, H. C. Kim and C. S. Hong, *Angew. Chem. Int. Ed.*, 2006, **45**, 7424; (*b*) J. H. Lim, H. S. Yoo, J. I. Kim, J. H. Yoon, N. Yang, E. K. Koh, J.-G. Park and C. S. Hong, *Eur. J. Inorg. Chem.*, 2008, 3428; (*c*) J. H. Lim, H. S. Yoo, J. H. Yoon, E. K. Koh, H. C. Kim and C. S. Hong, *Polyhedron*, 2008, **27**, 299; (*d*) M. G. Hilfiger, H. Zhao, A. Prosvirin, W. Wernsdorfer and K. R. Dunbar, *Dalton Trans*., 2009, 5155; (*e*) B. Nowicka, K. Stadnicka, W. Nltek, M. Rams and B. Sieklucka, *CrystEngComm*, 2012, **14**, 6559; (*f*) S. Chorazy, M. Reczyński, R. Podgajny, W. Nogaś, S. Buda, M. Rams, W. Nitek, B. Nowicka, J. Mlynarski, S. Ohkoshi and B. Sieklucka, *Cryst. Growth Des*., 2015, **15**, 3573.

18 (*a*) R. Podgajny, W. Nitek, M. Rams and B. Sieklucka, *Cryst. Growth Des*., 2008, **8**, 3817; (*b*) R. Podgajny, S. Chorazy, W. Nitek, M. Rams, M. Bałanda and B. Sieklucka, *Cryst. Growth Des*., 2010, **10**, 4693; (*c*) S. Chorazy, R. Podgajny, W. Nitek, M. Rams, S. Ohkoshi and B. Sieklucka, *Cryst. Growth Des*., 2013, **13**, 3036.

19 (*a*) J. An, Z.-D. Chen, J. Bian, J.-T. Chen, S.-X. Wang, S. Gao and G.-X. Cu, *Inorg. Chim. Acta*, 2000, **299**, 28; (*b*) R. Bagai and G. Christou, *Chem. Soc. Rev.*, 2009, **38**, 1011; (*c*) G. Redler, C. Lampropoulos, S. Datta, C. Koo, T. C. Stamatatos, N. E. Chakov, G. Christou and S. Hill, *Phys. Rev. B*, 2009, **80**, 094408; (*d*) Y.-Y. Zhu, T.-T. Yin, S.-D. Jiang, A.-L. Barra, W. Wernsdorfer, P. Neugebauer, R. Marx, M. Dörfer, B.-W. Wang, Z.-Q. Wu, J. van Slageren and S. Gao, *Chem. Commun.*, 2014, **50**, 15090.

20 (*a*) A. Samotus, *Pol. J. Chem.*, 1973, **47**, 653; (*b*) R. A. Pribush and R. D. Archer, *Inorg. Chem.*, 1974, **13**, 2556; (*c*) D. Matoga, J. Szklarzewicz and M. Mikuriya, *Inorg. Chem.*, 2006, **45**, 7100.

21 (*a*) A. Altomare, G. Cascarano, C. Giacovazzo and A. Guagliardi, *J. Appl Crystallogr.*, 1993, **26**, 343; (*b*) G. M. Sheldrick, *Acta Crystallogr.*, 2015, **C71**, 3; (*c*) C. F. Macrae, I. J. Bruno, J. A. Chisholm, P. R. Edgington, P. McCabe, E. Pidcock, L. Rodriguez-Monge, R. Taylor, J. van der Streek, P. A. Wood, *J. Appl. Crystallogr.*, 2008, **41**, 466.

22 G. A. Bain, J. F. Berry, *J. Chem. Educ.*, 2008, **85**, 532.

23 (*a*) M. Llunell, D. Casanova, J. Cirera, J. Bofill, P. Alemany, S. Alvarez, M. Pinsky and D. Avnir, *SHAPE v. 2.1. Program for the Calculation of Continuous Shape Measures of Polygonal and Polyhedral Molecular Fragments,* University of Barcelona: Barcelona, Spain, 2013; (*b*) D. Casanova, J. Cirera, M. Llunell, P. Alemany, D. Avnir and S. Alvarez, *J. Am. Chem. Soc.*, 2004, **126**, 1755.

24 F. Lloret, M. Julve, J. Cano, R. Ruiz-Garcia and E. Pardo, *Inorg. Chim. Acta*, 2008, **361**, 3432.

25 Y.-Q. Zhang and C.-L. Luo, *Inorg. Chem.*, 2009, **48**, 10486.

A table of content entry:

The solvent effect on the structural and magnetic features of bidentate ligand-capped {Co$^{II}_9$[W^V(CN)$_8$]$_6$} Single-Molecule Magnets

Szymon Chorazy, Anna Hoczek, Maciej Kubicki, Hiroko Tokoro, Shin-ichi Ohkoshi,* Barbara Sieklucka, and Robert Podgajny*

L$_1$ =　　　　L$_2$ = CH$_3$CN, CH$_3$OH, C$_2$H$_5$OH

Cyanido-bridged {Co$^{II}_9$W$^V_6$} clusters combined with 2,2'-bipyridine N-oxide produce three crystalline phases with different solvents affecting their structural and magnetic properties.